Optical Engineering

OpticalEngineering.SPIEDigitalLibrary.org

Achromatization method for multichannel fluorescence imaging systems

Michal E. Pawlowski
Yiran Yang
Cynthia Wong
Tomasz S. Tkaczyk

SPIE.

Michal E. Pawlowski, Yiran Yang, Cynthia Wong, Tomasz S. Tkaczyk, "Achromatization method for multichannel fluorescence imaging systems," *Opt. Eng.* **58**(1), 015106 (2019), doi: 10.1117/1.OE.58.1.015106.

Optical Engineering 58(1), 015106 (January 2019)

Achromatization method for multichannel fluorescence imaging systems

Michal E. Pawlowski,[a] Yiran Yang,[a,b] Cynthia Wong,[a] and Tomasz S. Tkaczyk[a,c,*]
[a]Rice University, Department of Bioengineering, Houston, Texas, United States
[b]California Institute of Technology, Department of Medical Engineering, Pasadena, California, United States
[c]Rice University, Department of Electrical and Computer Engineering, Houston, Texas, United States

Abstract. An achromatization method optimized for dual-channel imaging is developed. Dichroic mirrors are employed to split and recombine narrowband signals, and separation between catoptric components is used to minimize the longitudinal chromatic shift. An achromatic system based on this principle could be built from singlet lenses, since refractive element properties such as dispersion and power are not utilized to optimize wavelength-dependent performance. To demonstrate the validity of the proposed solution, a prototype miniature fluorescence microscope optimized for two emission lines of acridine orange (525 and 650 nm) is built. To reduce the cost and accelerate assembly, the system is built from commercially available optical components. The optical train consisted of two plastic singlet lenses combined with a pair of dichroic mirrors. Optical performance of the prototype is evaluated by imaging a bar line target at both design wavelengths. To demonstrate the potential of the proposed design strategy, the achromatic system prototype is used to measure a two-part white blood cells differential count on a venous blood sample. Data from the prototype fluorescence microscope are compared against results from a commercially available blood analyzer, and the difference between both instruments is within 20%. [DOI: 10.1117/1.OE.58.1.015106]

Keywords: fluorescence microscopy; optical design and fabrication; medical optics and biotechnology; diagnostic instrumentation.

Paper 181485 received Oct. 16, 2018; accepted for publication Dec. 28, 2018; published online Jan. 22, 2019.

1 Introduction

Optical systems are typically expected to meet stringent image quality metrics over a broad range of wavelengths. Achromats are the simplest optical components optimized for multispectral performance. In achromatic designs, the back focal plane positions are controlled at two selected spectral bands. Advanced apochromatic systems minimize the chromatic back focus variation in a secondary spectrum region, which is left uncorrected in achromatic designs. Because geometric and wavelength-dependent aberrations are typically corrected at the same time, construction of achromatic and apochromatic systems is difficult and various strategies have been developed over the years to address that problem.

Most commercially available achromatic systems are constructed by combining glasses with dissimilar dispersion properties. Usually, positive and negative lenses made out of two materials having different Abbe number are matched together. Typically, crowns are paired with flints, and a combination of two or more lenses is glued together to produce a robust, integrated component.[1] If the correction of geometric aberrations is critical from a performance stand-point, multilens achromatic systems may be mounted together with air-spaces, though such systems are typically sensitive to manufacturing and assembly tolerances.[1] Plastic optical materials can also be successfully combined together to form doublets,[2–4] and such systems are well suited for mass production due to scalability of an injection molding process. Hybrid glass and plastic achromatic systems built using the above-mentioned strategies have also been reported.[5] To overcome the linear relation limitation between Abbe number and relative partial dispersion seen in most glasses, heterogeneous glass–liquid–glass multilayered structures were developed to take advantage of the unique dispersion properties of liquids.[6,7] Independent from material choice, construction of achromatic lenses requires precise knowledge of the refractive index of constituent parts, and often systems need to be reoptimized for a specific batch of material(s), which make doublets more labor-intensive and expensive as compared with singlet lenses.

Recent progress in manufacturing technologies, specifically diamond turning and injection molding, allowed for the integration of diffractive optical elements (DOE) with lenses. Since the dispersion of diffractive components has an opposite sign to the dispersion of the bulk optical materials, a lens can be achromatized by careful numerical optimization of a diffractive pattern that is specifically tailored to a given working condition. Typically, mass-produced plastic components are achromatized this way due to the fact that the initial expensive injection mold price tag can be split across millions of copies.[8,9] The applicability of DOEs is limited by the efficiency of the diffractive structures, and typically, only one component in the optical train can be achromatized this way.[10] Alternatively, achromatic systems can be constructed from reflective components due to the wavelength-independent nature of the reflection angle. Thus, catoptric systems by definition are apochromatic in a range limited by the reflectivity of the material.[11] While catoptric systems can work in a broad spectrum range, systems achromatized that way are usually bulky and suffer from small field-of-view (FOV), and for that reason, reflective systems are mainly used to design astronomical

*Address all correspondence to Tomasz S. Tkaczyk, E-mail: ttkaczyk@rice.edu

0091-3286/2019/$25.00

telescopes or specialty objectives, such as photographic telephoto lenses or broadband microscope objectives.

Fluorescence microscopy revolutionized the biomedical diagnostic landscape by replacing morphological examination of images with simple and easy-to-automate analysis of intensity. Thanks to the progress in development of highly specific dyes with controllable chemical and optical properties, simultaneous observation of multiple target molecules becomes possible. Typically, information about concurring processes or molecules observed in parallel is encoded in spectrally separated fluorescence channels. Thus, fluorescence optical systems need to be achromatized to provide uniform performance across all spectral channels of interest. For example, dual-channel fluorescence microscopic system can be used for tissue diagnostic purposes by making use of metachromatic dyes such as toluidine blue.[12] Drug concentration levels can be monitored at the point-of-care settings by two-channel fluorescence systems utilizing bioluminescent sensor proteins.[13] Dual-channel fluorescence systems can be employed to delineate human leukemia types[14] and diagnose Creutzfeld–Jakob and Alzheimer diseases.[15]

In this paper, we describe a cost-effective achromatization method suitable for narrow-band multichannel imaging systems for point-of-care applications. The presented concept is used in a molecular detection digital microscope and allows for relaxed system requirements. Fluorescence microscopes in general need to include filters to separate the strong excitation signal from the much weaker emission signal. Since these filters are necessary, we decided to incorporate the filter into the optical design as a way to perform chromatic correction. By doing so, we allow for looser requirements in the design and application of single lens plastic components. The overall cost of such devices can be low and broadly deployed in a number of specialized applications at the point of care, including, for example, white blood cell (WBC) count and differential tests. Specifically, we propose to correct the axial chromatic shift between mutually exclusive, narrowband spectral signals by adjusting propagation path length for each channel individually. Longitudinal chromatic aberration is compensated by axial separation between dichroic mirror surfaces, which are used to split and recombine spectrally separated imaging channels. We demonstrate the feasibility of this solution through a custom compound microscope constructed from two singlet lenses and a pair of dichroic mirrors optimized for the emission lines of acridine orange (AO). To reduce the cost of the prototype, only commercially available components were used. We present a detailed description of the optomechanical design, report manufacturing steps, and evaluate the performance of the prototype. Because the catadioptric miniature microscope was built from two singlet lenses and two mirrors, the optical system was simple, which will translate in the future to low price of the final system. Additionally, since all components are commercially available, this would allow the device to be mass producible, further driving down the cost of the molecular detection–based imaging systems.

To demonstrate the viability of the microscope, we performed a two-part WBC differential count on a sample of whole venous blood. The WBC count is one of the most common blood tests and can be used, for example, to discern viral from bacterial infections. The metachromatic organic dye AO can be used to distinguish between different types of WBCs. When bound with DNA, AO fluoresces green (Ex. 502 nm, Em. 525 nm) and when bound with RNA, it emits in the red part of the spectrum (Ex. 460 nm, Em. 650 nm). Based on the ratio of intensity in these two emission channels, individual WBCs can be divided into agranulocytes and granulocytes. The cell count for each group together with their ratio is frequently used to diagnose overall patient condition, and in the case of infection can be used to identify its nature. The result obtained from the prototype of a miniature fluorescent microscope was compared against a commercially available hematology analyzer. To the best of our knowledge, this is the first publication to describe a multichannel achromatization strategy that allows separate correction of monochromatic and chromatic aberrations in a catadioptric system exclusively built from singlet lenses.

2 Optical Design

A schematic of an optical system illustrating the presented achromatization principle is shown in Fig. 1. A two element microscope built from a pair of singlet lenses with the optical path folded by a 45-deg mirror is depicted in Fig. 1(a). In this configuration, the images of an object for two mutually

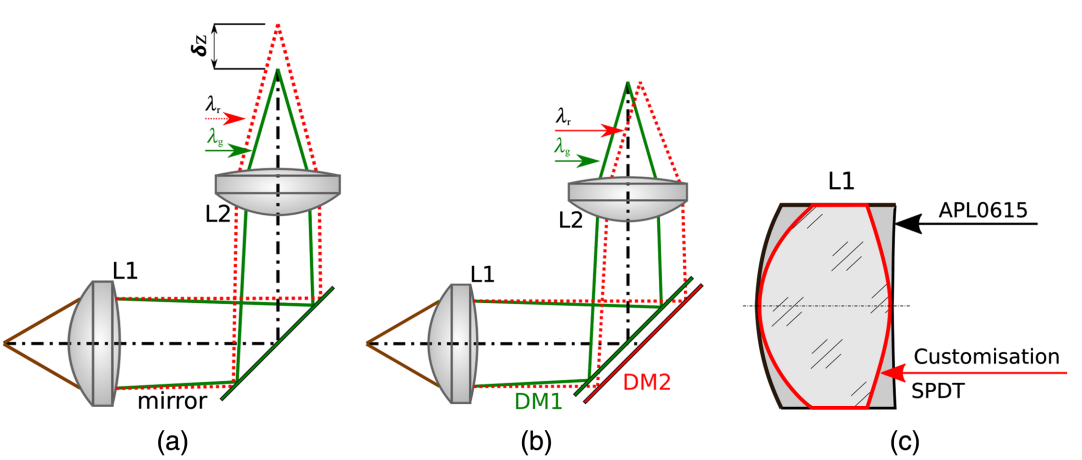

Fig. 1 (a) Schematic of a simple imaging system built from two singlet lenses with the optical path folded by a 45-deg mirror. (b) Optical schematic of a system achromatized using a set of two dichroic mirrors. (c) Cross-section through a stock APL0615 lens (black) and its customized form (red). L1, L2, lenses; DM1, DM2, dichroic mirrors; SPDT, single point diamond turning, $\lambda_g < \lambda_r$.

exclusive spectral channels centered at λ_r and λ_g (red and green lines, respectively, with $\lambda_g < \lambda_r$) are separated by an axial distance δ_z due to uncorrected chromatic aberrations induced by the lenses L1 and L2. To correct the chromatic shift between both images, we propose to replace the path-folding mirror with a set of two dichroic elements as schematically depicted in Fig. 1(b). The first dichroic mirror reflects the radiation centered at λ_g, for which the index of refraction of both singlet lenses L1 and L2 is higher and for which the working distance in the image space is shorter. The second dichroic mirror reflects light from the imaging channel centered at λ_r, for which the index of refraction of both singlet lenses is smaller and for which the working distance in the image space is longer. In this configuration, axial shift between both channels can be corrected by adjusting the axial separation between dichroic mirrors. The radii of curvature of lenses L1 and L2 together with the interelement distances can be used to further optimize system performance. The proposed achromatization method introduces a lateral chromatic image shift, which is proportional to the axial separation between the dichroic components. However, the lateral chromatic shift can be corrected numerically if the spectral channels centered at λ_r and λ_g can be separated, which can be achieved by employing a color-sensitive detector.

A fluorescent microscope optimized for a two-part WBC differential was built to demonstrate the applicability of the presented achromatization principle. The system was optimized for two emission lines of AO centered at 525 and 650 nm, respectively. The designed FOV had a diameter of 1 mm to acquire at least 100 WBCs within the measurement window of a custom cartridge[16] filled with undiluted blood. The minimum WBCs count was necessary to reach a clinically relevant coefficient of variation of 10%.[17] Image side NA was set to 0.25 to provide adequate resolution to distinguish the smallest leukocytes, which have an average diameter on the order of 7 μm, as well as to guarantee sufficient light collection efficiency to image the emitted fluorescence signal from AO. The working distance was constrained to 1 mm to allow for comfortable insertion and removal of test cartridges.

Commercially available components were used to reduce cost and speed-up construction of the prototype. A combination of components that met our initial requirements regarding FOV, magnification, and object space NA was identified using the built-in database of plastic/glass singlet objectives in Zemax (Radiant Vision Systems, Washington), together with online resources from major optics vendors (Edmund Optics, Thorlabs). In all tested combinations, two dichroic mirrors were placed between the microscope objective and the tube lens. Specifically, a short-pass dichroic beam splitter (FF611-SDi01-25x36, 611 nm, Semrock) and a long-pass dichroic beam splitter (FF593-Di03-25x36, 594 nm, Semrock) were modeled in a multiconfiguration system to enable correction of axial chromatism for 525- and 650-nm wavelengths. The working distance of the microscope objective and intercomponent separation together with image distance were used to optimize system performance. Distance between the dichroic mirrors in the 650 nm configuration was adjusted to correct for axial chromatic aberration. After sorting all tested combinations of lenses in ascending order of the on-axis root mean square (RMS) spot diameters, the combination of lenses that yielded the smallest RMS spot size consisted of a molded acrylic aspheric lens, $f = 15.12$ mm (APL0615, Thorlabs) working in tandem with an uncoated double-convex lens $f = 39.16$ mm (63540, Edmund Optics).

The shorter focal length lens served as a microscope objective, while the Edmund Optics lens worked as a tube lens. Using these stock lenses, the best system had an RMS wavefront error of 0.37 waves for both monochromatic configurations. Since the nominal performance of the system evaluated using RMS wavefront error was not satisfactory, we decided to customize the first lens by setting both radii and conic constants as variables. Care was taken during subsequent optimization iterations to make sure that the optimized lens shape could be manufactured using single-point diamond turning technology, i.e., the lens would be manufactured by removing material from the stock lens. Additional constraint parameters controlled the axial thickness and sag of both surfaces to ensure that the axial length of the cylindrical part of the modified lens would be longer than 1.5 mm to allow for robust mounting on the diamond turning lathe. After optimization, the stock concave–convex APL0615 lens was turned into a 3.85-mm long double convex lens with aspheric surfaces. A cross-sectional drawing showing the off-the-shelf APL0615 and its modified version is shown in Fig. 1(c). The envelope of the stock APL0615 lens is drawn using a black continuous line, and the red line depicts shape of the modified lens; the dark grayed areas on Fig. 1(c) mark the volume of the stock lens that was removed.

The optical prescription of the miniature achromatic dual-channel catadioptric microscope is shown in Table 1. The final system's Strehl ratio measured for an axial field point was equal to 0.88 and 0.95 for the 525- and 650-nm configurations, respectively. The nominal modulation transfer function plots for both monochromatic configurations are shown in Figs. 2(a) and 2(b) for green and red spectral channels, respectively, for axial and marginal field points. The field curvature plots for both sagittal and tangential points are shown in Fig. 2(c). Distortion plots for both configurations are depicted in Fig. 2(d). The diffraction-limited performance for the presented system was preserved within a centrally located 0.44-mm diameter disk. At the edge of the FOV (0.5-mm field point), the RMS spot diagram radius had the largest value and was 2.1 and 1.6 times larger than the Airy disk radius for the 525- and 650-nm configurations, respectively. Sagittal field curvatures for both design wavelengths were above the systems depth of focus (0.22 mm for the shorter design wavelength). The field curvature was left uncorrected due to the limited ability to introduce elements with negative power, physical component separation constraints, and the overarching goal of simplifying the system optomechanical design. Distortion had a negative sign for both configurations, suggesting barrel-type geometric deformation, which was negligible for our application amplitude below −0.3%. Since the system was nominally diffraction limited at the optical axis (resolution of 1.05 and 1.25 μm for 525- and 650-nm bands, respectively) and would reach a resolution of 2.7 and 2.8 μm at the edges of the FOV for 525- and 650-nm configurations, respectively, the minimum resolution criterion was met for all field points. Since the presented achromatization method

Table 1 Optical prescription of a miniature achromatic dual-channel catadioptric microscope optimized for 525- and 650-nm wavelengths. Values in curly braces are for values from the 650-nm configuration.

Radius (mm)	Thickness (mm)	Material	Diameter	Conic	Comment
∞	3		0.500		Object
4.232	3.850	PMMA	6.000	−8.133	Custom-modified APL0615
−2.977	7.526		6.000	−0.870	
∞	0	{BK7}	{4.000}		Conf #1 (525 nm)
	{1.100}				{Conf #2 (650 nm)Dichroic mirror #1}
∞	0		{4.000}		Conf #1 (525 nm)
	{1.037}				{Conf #2 (650 nm)Dichroic mirror #1}
		Mirror	4.000		Conf #1 (525 nm)
		{Mirror}	{4.000}		{Conf #2 (650 nm)Dichroic mirror #1}
∞	0		{4.000}		Conf #1 (525 nm)
	{−1.037}				{Conf #2 (650 nm)Dichroic mirror #1}
∞	0	{BK7}	{4.000}		Conf #1 (525 nm)
	{−1.10}0				{Conf #2 (650 nm)Dichroic mirror #1}
∞	−7.526		4.000		
−40.910	−2.500	BK-7	5.000		EO #63–540
40.910	−12.752		5.000		
∞			2.808		Image

relies on the introduction of spectrally optimized focusing distance, it cannot be used in an infinity corrected microscope configuration. While the starting configuration for all combinations of tested lenses was deliberately chosen to be an infinity corrected compound microscope, the distance between the tube lens and the microscope objective was used as one of the optimization variables.

The achromatization approach presented in this paper enables correction of axial chromatism, but due to axial separation between mirrors induces lateral chromatism. Lateral chromatic aberration, schematically depicted in Fig. 1(b), cannot be optically corrected in a system assembled from two singlet lenses. However, the two emission lines of AO can be separated directly by red and green filters of a Bayer mask RGB camera, because the emission line of AO centered at 525 nm overlaps with the spectral sensitivity of green Bayer mask filters and the 650-nm emission line falls within the spectral sensitivity range of red Bayer mask filters. In general, central wavelengths of optimized channels do not have to overlap with the spectral sensitivity of the image detector color channels. Alternatively, the problem of spectral separation can be solved by taking advantage of a hue–saturation–Luma (HSL) rather than an RGB color model. In the HSL space, mutually separated emission lines can be identified in two-dimensional hue–saturation space, whose extent is limited by the spectral sensitivity of a detector. Spectrally separated and laterally shifted images can be later electronically overlaid using geometric transformations into a composite two-channel image. Lateral chromatic shift in the presented system for a marginal field point was equal to 232 μm. Note that in general one needs to control the magnitude of the lateral chromatic shift, as it reduces the overlapping area between two spectrally separated images. The main parameters of the prototype are assembled in Table 2.

3 Optomechanical Design and Prototype Evaluation

The optomechanical schematic of the miniature catadioptric fluorescent microscope prototype is shown in Fig. 3. The exploded view of the system with major parts labeled is depicted in Fig. 3(a). The cross-sectional view through the assembled system showing lens ports and mounting features is shown in Fig. 3(b). The system chassis together with lens mounts and spacers were designed in SolidWorks (Dassault Systèmes, France).

Mechanical components were manufactured on a ProJet SD3000 3-D printer (3-D Systems) from UV curable epoxy. A spacer placed between the dichroic mirrors was originally 3-D printed but later was replaced by spacers made from paper, as the 3-D printed component did not meet expected dimensional tolerances. The APL0615 polymer lens was customized on an Optimum 2400 diamond turning lathe (Precitech), and the NanoCam2D software (Moore Tools) was used to automatically generate a tool path based on the Zemax model. Microscope assembly was performed

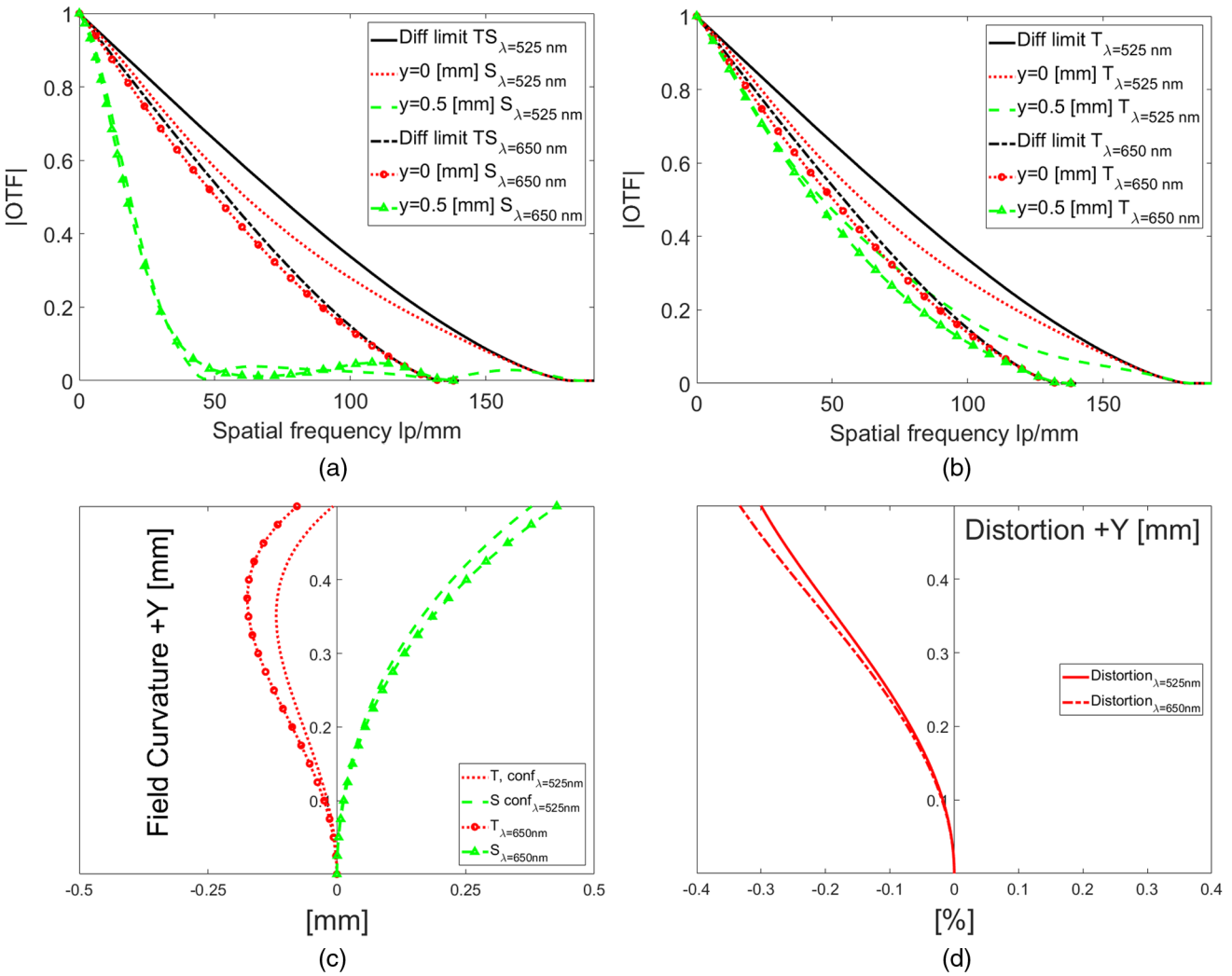

Fig. 2 Modulus of the optical transfer function for axial and marginal field points for 525- and 650-nm wavelengths. Tangential plots and sagittal plots are given in (a) and (b), respectively. (c) Field curvature for both configurations for tangential and sagittal planes. (d) Distortion for green and red configuration.

Table 2 Optical parameters of the miniature microscope.

Object space NA	0.25
Magnification	5.15×
Field of view	1 mm (diameter)
Working distance	3.0 mm
Dichroic mirror separation	1.037 mm
Total length of optical system	41.423 mm
Design wavelength	525 and 650 nm

with compression mounting using six flat head screws. Metal nuts and screws were used because the mechanical properties of 3-D printed parts were not conducive to designs featuring snap-like dismountable components, and printed threads did not have enough mechanical strength to support multiple mount-dismount cycles required at the prototype stage. A picture of the assembled microscope is shown in Fig. 3(c) with a one cent coin for size comparison. In all experiments, a Flea3 color camera (FL3-U3-88S2C, FLIR) served as an image detector, and the manufacturer-provided FlyCapture2 (FLIR) program was used to acquire images in a raw, non-demosaicked format.

The optical performance of the prototype was tested using a 1951 United States Air Force (USAF) resolution target. To simulate the emission spectra of AO, tests were performed using two narrowband filters centered at 520 nm (EO #65-639) and 650 nm (EO #65-655), which were successively placed into the optical train of the imaging system. The images of the USAF bar test captured for red and green channels are shown in Figs. 4(a) and 4(b), respectively. Subimages (a) and (b) represent raw intensity samples that were not modified by application of the demosaicking filter, which is typically used to provide continuous and equally spaced distribution of spectrally separated intensity samples. A composite representation of the test object is shown in Fig. 4(c). Input images were combined by means of a custom script developed in MATLAB (MathWorks), which shifted one of the images by the operator-selected vector $\langle \Delta x, \Delta y \rangle$ before combining them together.

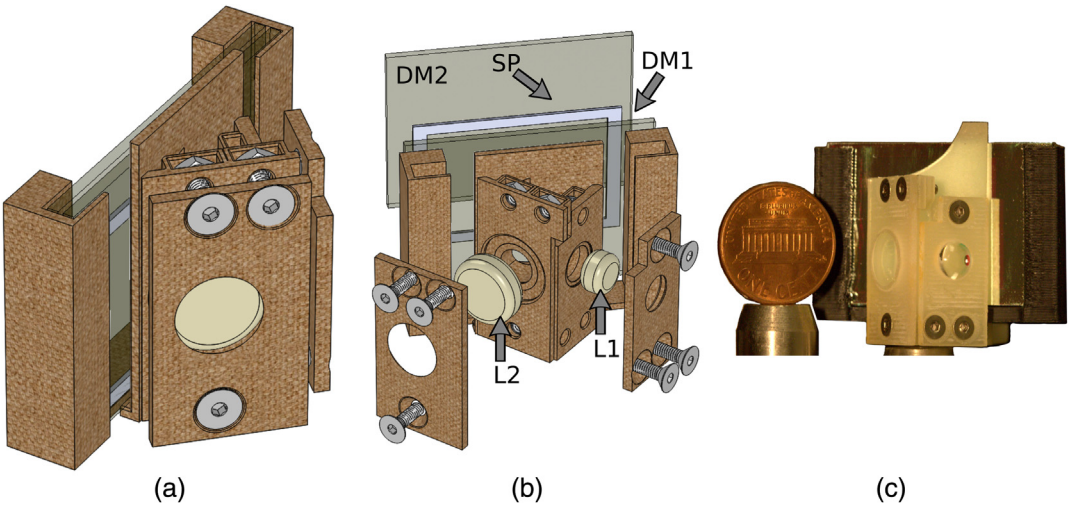

Fig. 3 (a) Optomechanical model of the miniature dual-channel achromatic catadioptric microscope prototype. (b) Exploded view of the achromatic microscope assembly model. (c) Photograph of the assembled prototype with a one cent coin for scale comparison. L1 and L2, lens one and two, respectively; SP, spacer; DM1 and DM2, dichroic mirrors.

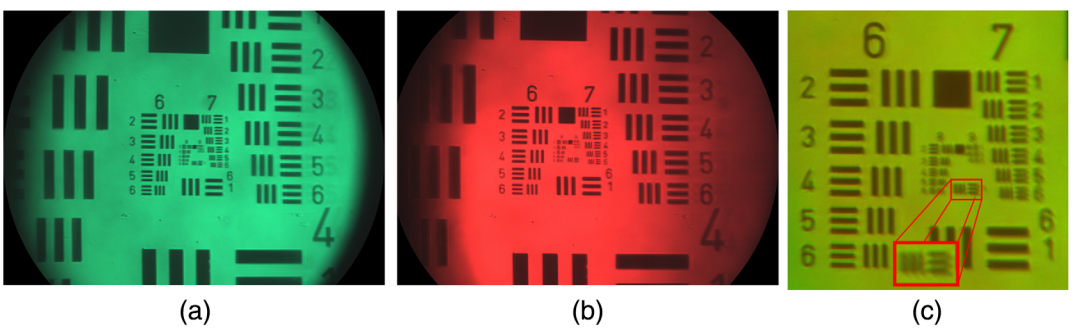

Fig. 4 Image of the 1951 USAF resolution target recorded by the miniature achromatic catadioptric fluorescence microscope through (a) 520 nm and (b) 650 nm narrowband filters. (c) Composite, dual-channel image of the resolution target reconstructed from narrowband subimages with magnified details of elements from group 8.

The smallest resolvable features within the composite image were part of group 8 element 1, which corresponds to a resolution of 256 lp/mm. A magnified version of group 8 element 1 is given in the inset of Fig. 4(c) (center bottom). The measured FOV had a 0.85-mm diameter, and at tested conjugates, the system reached a 5.2× magnification. According to the Rayleigh criterion, a diffraction-limited system at 650 nm working at an NA of 0.25 should resolve element 2 from group 9. The measured resolution was below nominal, but was better than the minimum required for the application. We attribute the theoretically predicted and experimentally measured resolution discrepancy to the structural imperfections of the enclosure. To minimize system footprint, thin-walled components were utilized across the mechanical design, and during postprocessing operations (oil and detergent baths applied to remove support material), these components warped and negatively affected alignment. Additionally, due to limited access to specialized metrology equipment, the distances between both lenses and dichroic mirrors was not verified and could be potentially off nominal values. The measured FOV was smaller than theoretically predicted (73% of the nominal FOV) due to the size of the Flea3 detector and was not limited by the optical system itself. The FL3-U3-88S2C camera was used because of its pixel size, application-appropriate spectral sensitivity, and low noise. While the reduced FOV will have an impact on the total cell count, according to the experimental data[17] it was predicted that at least 110 leukocytes would be visualized, a count slightly above the minimum required (of at least 100).

4 Two-Part White-Blood Cell Count Experiment

To experimentally verify the system performance, a sample of whole blood was deposited into the input port of a disposable cartridge and was subsequently stained with AO. The sample preparation and imaging procedures were identical to those described in previous publications.[4,17] The illumination system consisted of a 470-nm LED and an excitation filter (FF01-470/28-25, Semrock). An example composite image of whole blood stained with AO is shown in Fig. 5.

For each WBC in the image, the red-to-green (RG) ratio was calculated and the results were plotted on a histogram. This RG ratio histogram was later used to separate the agranulocytes (that tended to have a stronger green signal and thus a lower RG ratio) from the granulocytes (that tended to have a stronger red signal and thus a higher RG ratio).

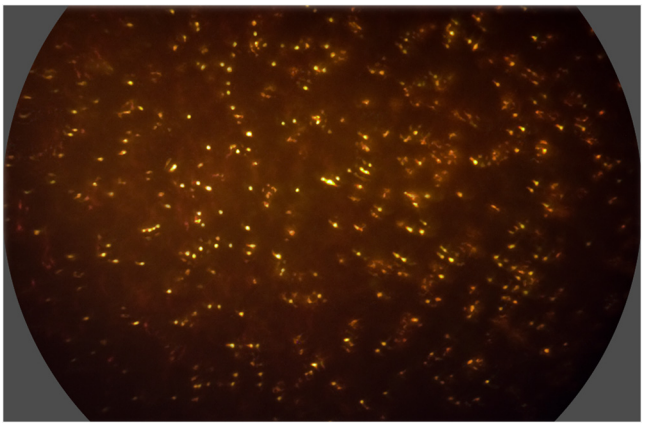

Fig. 5 Composite image of WBCs stained with AO. Image was cropped to remove nonused area of imaging sensor. Contrast was numerically enhanced for visualization purposes.

Table 3 Comparison of the differential WBC count as calculated for the prototype achromatic microscope to the gold standard reported by the commercial hematology analyzer.

Measurement	Achromatic microscope	Hematology analyzer
WBC (mL^{-1})	7.6	6.4
Agranulocytes (%)	31.4	37.6
Granulocytes (%)	68.6	62.4

A detailed description of the algorithm together with calibration procedures are provided in previous papers.[4,16,18,19] The overall concentration of WBCs was found by dividing the total number of WBCs by the sample volume. The results of the WBC counts are summarized in Table 3. The reported WBC counts were the average values of three FOVs from the same sample cartridge. These values were compared with the gold standard results from a commercial AcT Diff2 hematology analyzer (Beckman Coulter) and fell within 20% of the reference value. To meet Clinical Laboratory Improvement Amendments requirements, our results would have to be within 15% from the reference standard instrument. The difference between the standard and presented measurements can be reduced by improvements to both hardware and software. Since the WBCs count coefficient of variation depends on the number of WBCs within the field of view, the increase of the former at identical blood concentration levels should improve results. Additionally, further improvements to the system (such as a chassis with enhanced rigidity) and the collection of additional experimental data can contribute to improved repeatability and robustness of the data processing algorithm.

5 Future Development Directions

The optical system presented in this paper and depicted in Fig. 3(c) constitutes the simplest form of an achromatic catadioptric imaging system in which chromatic longitudinal aberration is compensated by axial separation of dichroic mirrors. The presented system incorporates two spectrally encoded mirrors, shown in Fig. 6(a), while in general, a production type system based on this principle could potentially utilize a double-coated dichroic mirror, as shown in Fig. 6(b). The use of an integrated component has a few advantages. From the optomechanical perspective, the separation between the two surfaces and their relative spatial orientation can be more tightly controlled for in a single glass substrate, in contrast to positioning a pair of mirrors. The price of a double-sided dichroic component may be competitive to a set of two off-the-shelf mirrors because optical coating jobs are typically quoted per process and not per part(s). Since the surface area of an integrated double-sided dichroic mirror can be optimized for a specific application (in the presented system, it could be reduced to ~4.2 mm in diameter), one may manufacture simultaneously tens of these components in a single process.

The presented achromatization strategy may be used to optimize three or more spectral channels by building sandwich-like structures from dichroic mirrors, schematically shown in Fig. 6(c). While the unwanted lateral chromatic aberration introduced by a set of axially separated dichroic mirrors cannot be corrected optically in the system schematically shown in Fig. 1(b), by use of a secondary set of complementary dichroic mirrors one may try to minimize both lateral and longitudinal chromatic shift, as schematically shown in Fig. 6(d). We would like to emphasize that in the presented achromatization method, axial chromatic aberration can only be corrected for in a narrow range of wavelengths for which longitudinal chromatic shift is within the

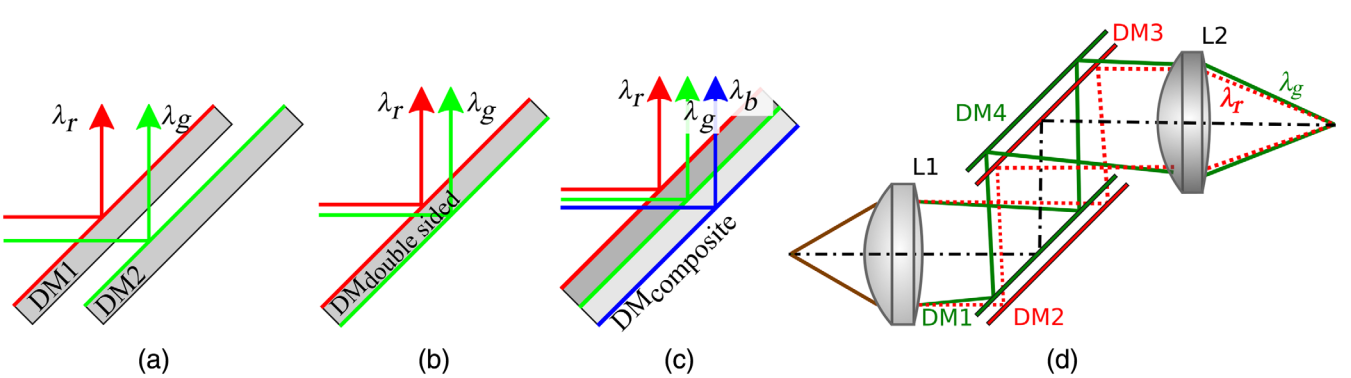

Fig. 6 Subsystem of (a) a dual-channel achromatic catadioptric system utilizing two separate dichroic mirrors and (b) a single-double-side coated dichroic mirror. (c) Conceptual rendering of a composite dichroic mirror optimized for three imaging channels. Optical schematic of a system for which both lateral and axial chromatic aberration can be corrected using the proposed achromatization principle.

system's depth of field. As a result, broadband performance is highly dependent on the dispersive properties of the utilized glass, and materials with high Abbe number such as CaF_2, MgF_2, MgF_2, and phosphate-type crowns should be used to minimize secondary chromatic aberration. Since those materials typically have a very low index of refraction, to control system aberration one should minimize the power of these components. As an induced lateral chromatic aberration results in nonsymmetric propagation of rays for all field points, correction of off-axis aberrations such as coma and astigmatism may be difficult.

The presented achromatization method best serves applications requiring a fixed number of narrowband channels, such as fluorescence-based diagnostic imaging of WBCs stained with AO, and is not intended to be applied in systems requiring broadband optimization of a continuous spectral range. Taking the above into consideration, the intended use of the proposed solution is in low NA, small magnification imaging systems optimized for a fixed number of imaging channels, for which diffraction-limited performance is not critically important, and cost, size, and optomechanical simplicity is advantageous.

6 Conclusions

An achromatization methodology for catadioptric systems was developed. A prototype of a miniature, spectrally corrected microscope was developed using off-the-shelf commercially available components. The optical path of the prototype was folded by 90 deg by a set of two dichroic mirrors, where axial separation was used to correct longitudinal chromatic shift of the image plane. The system performance was optimized for two channels, which covered the emission lines of AO. Possible modifications of the proposed achromatization principle were discussed, including utilization of custom double-sided dichroic mirrors and multilayer stacks of single-sided dichroic mirrors. Limitations of the proposed solution together with suggested ways to optimize both lateral and axial chromatic shifts were also discussed. The presented achromatization principle is compatible with contemporary large-scale production processes, and even for short production runs, custom dichroic mirrors deposited on glass/plastic substrates may present a financially viable option. In the experimental system presented above, a set of two dichroic mirrors was used to optimize spectral performance. For short-scale and serial production, the two dichroic components can be replaced by a single mirror in which dimensions and custom coatings deposited on opposing sides will provide similar functionality. Although the system presented in this paper was optimized for a fixed pair of fluorescence channels, we believe that it is possible to construct a universal system around a set of swappable dichroic modules to optimize performance for multiple combinations of fluorophores, albeit working distances would probably need to be adjusted. Additionally, custom dichroic coatings may also provide the same functionality normally reserved for emission filters, further simplifying the system layout.

A WBC differential count experiment successfully demonstrated the usability of the proposed achromatization solution in a clinically relevant test. The results obtained from the prototype were compared with a reference blood analyzer and were within 20% of the reference values, which we believe could be improved in the future by further development of the system, namely modification of the field of view, chassis improvement, and data processing algorithm updates. Finally, we would like to emphasize that the proposed achromatization solution together with the selected manufacturing strategy allowed us to build a functional prototype in a very short time frame of a few weeks. In the future, we plan to develop more systems based on the presented achromatization principle with a focus on low cost, robust diagnostic imaging.

Acknowledgments

This work was financially supported by generous grants provided by NIH R21EB016832 and R01CA186132. We would like to thank Catherine Majors from Rebecca Richards-Kortum's laboratory for preparing initial blood samples. Additionally, we would like to thank Jason Dwight for fruitful discussions and help in the preparation of this paper. Authors do not have relevant financial interests in this paper. Tomasz S. Tkaczyk has financial interests in Attoris LLC focusing on hyperspectral technologies.

References

1. M. J. Kidger, *Fundamental Optical Design*, SPIE Press, Bellingham, Washington (2002).
2. M. Kyrish et al., "Achromatized endomicroscope objective for optical biopsy," *Biomed. Opt. Express* **4**(2), 287–297 (2013).
3. G. C. Birch et al., "Hyperspectral Shack-Hartmann test," *Appl. Opt.* **49**(28), 5399–5406 (2010).
4. A. Forcucci et al., "All-plastic, miniature, digital fluorescence microscope for three part white blood cell differential measurements at the point of care," *Biomed. Opt. Express* **6**(11), 4433–4446 (2015).
5. I. D. Nokolov et al., "Hybrid plastic-glass optical systems," *Proc. SPIE* **3430**, 61–68 (1998).
6. R. D. Sigler, "Apochromatic color correction using liquid lenses," *Appl. Opt.* **29**(16), 2451–2459 (1990).
7. R. D. Sigler, "Designing apochromatic telescope objectives with liquid lenses," *Proc. SPIE* **1535**, 89–112 (1991).
8. C. Landoño et al., "The design of achromatized hybrid diffractive lens system," *Proc. SPIE* **1354**, 30–38 (1991).
9. T. Nakai et al., "Research on multi-layer diffractive optical elements and their application to camera lenses," in *OSA Trends Opt. and Photonics Ser. Proc.* (2002).
10. R. Fischer et al., *Optical System Design*, McGraw-Hill, New York (2000).
11. W. J. Smith, *Modern Lens Design*, McGraw-Hill, New York (2005).
12. S. Maxwell and D. Hamerman, "Metachromasia; chemical theory and histochemical use," *J. Histochem. Cytochem.* **4**(2), 159–189 (1956).
13. G. Rudolf et al., "Bioluminescent sensor proteins for point-of-care therapeutic drug monitoring," *Nat. Chem. Biol.* **10**(7), 598–603 (2014).
14. M. Andreeff et al., "Discrimination of human leukemia subtypes by flow cytometric analysis of cellular DNA and RNA," *Blood* **55**(2), 282–293 (1980).
15. J. Bieschke et al., "Ultrasensitive detection of pathological prion protein aggregates by dual-color scanning for intensely fluorescent targets," *Proc. Natl. Acad. Sci. U.S.A.* **97**(10), 5468–5473 (2000).
16. C. E. Majors et al., "Low-cost disposable cartridge for performing a white blood cell count and partial differential at the point-of-care," in *IEEE Healthcare Innov. Conf.*, pp. 10–13 (2014).
17. H. M. Shapiro, "'Cellular astronomy': a foreseeable future in cytometry," *Cytom. Part A* **60A**, 115–124 (2004).
18. C. E. Majors et al., "Imaging based system for performing a white blood cell count and partial differential at the point of care," in *Clin. and Transl. Biophotonics*, Optical Society of America (2016).
19. C. E. Majors et al., "Low cost imaging based device for performing a white blood cell count and 3-part differential at the point of care," *Am. J. Trop. Med. Hyg.* (95), 70–71 (2017).

Michal E. Pawlowski is a research scientist at the William Marsh Rice University at Bioengineering Department. He received his MSc Eng degrees in optics from Warsaw University of Technology in 1997 and his PhD in optics from Warsaw University of Technology in 2002. He is the author of more than 58 publications and is the coauthor of eight patents. His current research interests include optical instrumentation, 3D printing of optical components, and optical design.

Yiran Yang is currently a graduate student in the Department of Medical Engineering, California Institute of Technology. She received her BS degree in bioengineering from Rice University in 2017. Her current research interests include biomedical optical system and medical device. She is a member of Tau Beta Pi Engineering Society.

Cynthia Wong received her bachelor's degree from the University of Pittsburgh in the Department of Bioengineering in 2014. She is a PhD candidate in the Modern Optical Instrumentation and Bio-imaging Laboratory at Rice University in the Department of Bioengineering. Her current research focuses on developing optical diagnostic and detection tools for point-of-care settings.

Tomasz S. Tkaczyk received his MS and PhD degrees from the Institute of Micromechanics and Photonics, Warsaw University of Technology. He is an associate professor of bioengineering and electrical and computer engineering at Rice University. His research is in microscopy, endoscopy, cost-effective high-performance optics for diagnostics, and snapshot imaging systems. In 2003, he began working as a research professor at the College of Optical Sciences, University of Arizona. He joined Rice University in 2007.